Open

Light: Science & Applications (2013) 2, e78; doi:10.1038/lsa.2013.34

www.nature.com/lsa

ORIGINAL ARTICLE

The magnetic response of graphene split-ring metamaterials

Nikitas Papasimakis[1], Sukosin Thongrattanasiri[2], Nikolay I Zheludev[1,3] and FJ García de Abajo[1,2,4]

Graphene has emerged as a promising platform for THz plasmonics, allowing high confinement, long lifetimes and fast electrical tunability. Here, we predict a strong magnetic dipole response by graphene split nanorings at THz frequencies, allowing the attainment of metamaterials with a high degree of field confinement (approximately one hundredth of the excitation wavelength) that is not reachable with conventional noble metals. The magnetic response of highly doped graphene split-rings in the far-infrared is much stronger than that displayed by gold structures of similar thicknesses. We further explored stacked graphene layers as a practical way of producing high-frequency magnetism in thin, electrically tunable metamaterials. Our results support the great potential of using graphene to achieve electrically tunable magnetic metamaterials.
Light: Science & Applications (2013) **2,** e78; doi:10.1038/lsa.2013.34; published online 5 July 2013

Keywords: artificial magnetism; graphene; graphene plasmons; metamaterials; plasmonics

INTRODUCTION

The last decade has witnessed a vast body of literature on optical metamaterial designs that defy common intuition with achievements such as negative refraction[1] and magnetic response at high frequencies,[2,3] as well as promising applications for perfect lensing,[4] invisibility cloaks[5] and magnetic resonance imaging.[6] In many studies, split-rings have become a central element because they are capable of supporting strong induced currents, leading to a resonant magnetic response down to the near infrared.[7] Split-ring resonances can be driven by the excitation of plasmons that propagate along the ring circumference, particularly when its length is of the order of half the plasmon wavelength. This condition leads to the formation of a standing wave that is similar to that of a dipole antenna, as recently demonstrated by electron energy-loss spatially resolved spectroscopy.[8]

The performances of metamaterials are hampered by optical losses and by the lack of fast means to tune their spectral response. In this context, the potential of graphene as a novel plasmonic material has been considered[9,10] because of two important properties that are advantageous for metamaterial design: (i) graphene plasmons have short wavelengths compared to the excitation wavelength[11,12] and (ii) the frequencies of these plasmons can be electrically tuned by injecting charge carriers into the carbon sheet.[13–17] Experimental evidence of these two properties has been recently obtained by spatially mapping localized optical modes in graphene ribbons.[18,19] Thus, graphene split-rings (GSRs) are expected to display resonances for small sizes compared with traditional noble-metal split-rings. In addition, metamaterials formed by GSRs inherit the tunability of their atomically thin fabric.

In this paper, we investigate the magnetic response of GSRs. Specifically, we show that GSRs of suitable nanoscale dimensions can be used to produce strong magnetic responses under excitation by the electric field of an incident electromagnetic wave in the THz regime. Our results are supported by analytical theory and numerical electromagnetic simulations with the behavior of graphene described through its dynamic sheet conductivity. The latter can be approximated with the Drude model, which is robust in the low-frequency and strong-doping regimes,[18]

$$\sigma(\omega)=\frac{ia}{\omega+i\gamma} \tag{1}$$

where $a=e^2|E_F|/\pi\hbar^2$ is a constant with units of length/(time)^2 and is proportional to the Fermi energy E_F. The latter is defined with respect to the so-called Dirac point and depends on the charge carrier concentration n as $|E_F|=\hbar v_F\sqrt{\pi|n|}$. Here, $v_F\approx10^6$ m s^{-1} is the Fermi velocity. The damping rate γ is estimated from the DC mobility μ as $\gamma=ev_F{}^2/\mu E_F$ (e.g., $\hbar\gamma=1.3$ meV for $\mu=10\,000$ cm^2 V^{-1} s^{-1} and $E_F=0.5$ eV). Lastly, due to the relatively large size of the GSR resonators (GSRRs), the scattering effects at the edges can be neglected.[20]

METHODS

Figure 1a shows a characteristic GSR of diameter $D=1$ μm. We focused on normal-incidence excitation where the electric field is

[1]Optoelectronics Research Centre and Centre for Photonic Metamaterials, University of Southampton, Southampton, UK; [2]IQFR – CSIC, Serrano 119, 28006 Madrid, Spain; [3]Centre for Disruptive Photonic Technologies, Nanyang Technological University, Singapore; and [4]ICFO–Institut de Ciencies Fotoniques, Mediterranean Technology Park, 08860 Castelldefels (Barcelona), Spain
Correspondence: Dr N Papasimakis, Optoelectronics Research Centre and Centre for Photonic Metamaterials, University of Southampton, Southampton SO17 1BJ, UK.
E-mail: np3@orc.soton.ac.uk
Or Professor FJ García de Abajo, IQFR – CSIC, Serrano 119, 28006 Madrid, Spain.
E-mail: j.g.deabajo@nanophotonics.es
Received 23 September 2012; revised 11 January 2013; accepted 21 January 2013

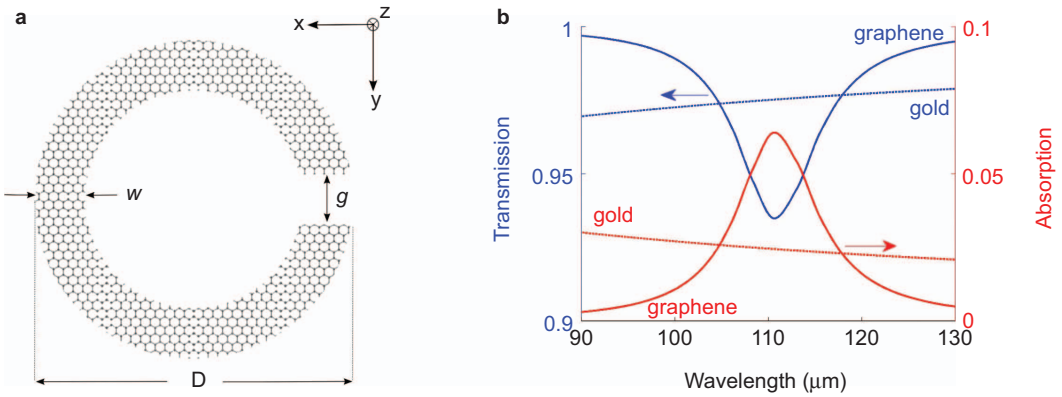

Figure 1 (**a**) A GSR resonator with diameter *D*, width *W* and gap distance *g*. (**b**) The normal-incidence transmittance (blue) and absorbance (red) spectra of a square split-ring array on monolayer graphene (solid curves) and monolayer gold (dotted curves). The geometrical parameters of the metamaterial array are $W=g=D/10$ with $D=1$ μm for graphene and $D=8.19$ μm for gold. According to Equation (7), the parameters yield resonance values within the same frequency range. The lattice spacing is $2D$ for both cases. Graphene is described by a Drude model with a Fermi energy of $E_F=0.5$ eV and a damping constant of $\gamma=1$ meV. Gold is described by its bulk parameters, assuming a thickness equal to the distance between the (111) atomic planes ($t=0.29$ nm). The incident-field polarization is across the gap (*y* direction). GSR, graphene split-ring.

polarized across the GSR gap (*y* direction). This configuration produces an electric dipole along the external field direction and a current circulating around the ring. The latter generates a magnetic dipole perpendicular to the ring (*z* direction). The coupling to the ring is maximum at a wavelength ~110 μm (>>*D*), as indicated by the GSR resonance feature observed in the simulated transmission and absorption spectra of Figure 1b, which were obtained by using a finite-element commercial code. Despite the small (compared to the excitation wavelength) size of the GSR resonators and the atomic thickness, the metamaterial presented clear resonant spectral features with transmission declining to 94% and absorption reaching 6%.

To understand the GSR response, we derived analytical expressions for the polarizability of a thin split-ring. Considering the small size of this structure compared with the excitation wavelength, we could work within the electrostatic approximation in which the self-consistent potential acting on the graphene is given by

$$\phi\left(\vec{\theta}\right)=\phi^{\text{ext}}\left(\vec{\theta}\right)+\eta\int\frac{d^2\vec{\theta}'}{|\vec{\theta}-\vec{\theta}'|}\nabla'\cdot f\left(\vec{\theta}'\right)\nabla'\phi\left(\vec{\theta}'\right) \qquad (2)$$

where ϕ^{ext} is the externally applied potential, f is 1 in the graphene area and 0 elsewhere,[21] and the integral term represents the Coulomb potential produced by the induced charge. The latter is from the continuity equation in terms of the divergence of the induced current, and this is in turn given by the gradient of ϕ. We used dimensionless spatial units $\vec{\theta}=(x/D,y/D)$ in the plane of the graphene. Equation (2) is also useful to study inhomogeneously doped graphene, with f proportional to the local Fermi energy.[21] We considered normally incident far-infrared radiation linearly polarized along y so that the external potential became $\phi^{\text{ext}}\left(\vec{\theta}\right)=-\theta_y DE^{\text{ext}}$. Importantly, the frequency dependence and the response of the graphene were fully contained inside the dimensionless parameter $\eta=i\sigma(\omega)/\omega D$. Incidentally, when graphene was placed at the interface between two dielectrics of permittivities ε_1 and ε_2, these expressions remain valid if we multiplied η by $2/(\varepsilon_1+\varepsilon_2)$.[22] In matrix notation, Equation (2) reduced to $\phi=\phi^{\text{ext}}-\eta M\varphi$, where $M=-|\vec{\theta}-\vec{\theta}'|^{-1}\nabla'\cdot f\left(\vec{\theta}'\right)\nabla'$ is a Hermitian operator.[23] It is convenient to expand the potential in terms of the eigenvectors of M plasmon resonances that emerge under the condition that $1/\eta$ equals one of the real eigenvalues of this operator, $1/\eta_p$. Using Equation (1), the corresponding plasmon energy was $\omega_p-i\gamma/2$, where

$$\omega_p=\sqrt{\frac{a}{\eta_p D}} \qquad (3)$$

The spectral width of the plasmon features was then identical with the intrinsic damping rate γ. This result is consistent with the resonance observed in Figure 1b, which has a quality factor $Q=\omega_p/\gamma\approx\lambda/\Delta\lambda\approx 11$. Lastly, we obtained the relevant elements of the polarizability tensor from the expressions

$$\alpha_{yy}^{EE}=\frac{iD^2}{\omega E^{\text{ext}}}\int d^2\vec{\theta}\, j_y^{\text{ind}} \qquad (4a)$$

$$\alpha_{zy}^{ME}=\frac{iD^3}{2cE^{\text{ext}}}\int d^2\vec{\theta}\left(\theta_x j_y^{\text{ind}}-\theta_y j_x^{\text{ind}}\right) \qquad (4b)$$

where j^{ind} was the induced surface current density in the graphene and the superscripts E and M stand for the electric and magnetic components, respectively. The induced current distribution is shown in Figure 2a at the resonance frequency, with the maximum values in the region opposite of the gap. Inserting the noted eigenmode expansion in Equation (4) and assuming a dominant split-ring plasmon mode, we find

$$\alpha_{yy}^{EE}\approx D^3\left[B^E+A^E\frac{\omega_p^2}{\omega_p^2-\omega(\omega+i\gamma)}\right] \qquad (5a)$$

$$\alpha_{zy}^{ME}\approx -iD^3\left(\frac{\omega D}{2c}\right)\left[B^M+A^M\frac{\omega_p^2}{\omega_p^2-\omega(\omega+i\gamma)}\right] \qquad (5b)$$

where $A^{E,M}$ and $B^{E,M}$ are real dimensionless constants that only depend on the geometrical aspect ratios (i.e., g/D and W/D, see Figure 1a) and ω_p is given by Equation (3). The resonances beyond the frequency range of interest contributed to a smooth background that was captured by $B^{E,M}$. From the reciprocity theorem, we found that $\alpha_{yz}^{EM}=-\alpha_{zy}^{ME}$. All of the other components of α were non-resonant; therefore, we dismissed them. In particular, the polarization produced by an external field directed perpendicular to the gap [along *x*, see Figure 1a] only produced marginal non-resonant absorption at levels <0.1%. To quantify the strength of the magnetic and electric responses of the GSR resonator array, we introduced the

doi:10.1038/lsa.2013.34

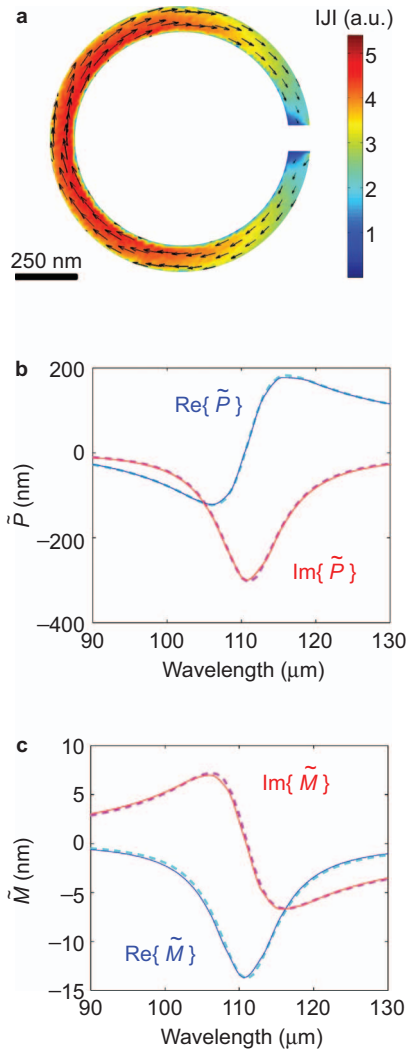

Figure 2 (**a**) The on-resonance induced current in a GSR under the conditions described in Figure 1b. (**b**, **c**) The electric ($\tilde{P}$) and magnetic ($\tilde{M}$) polarizability densities: full simulation (solid curves) compared with the analytical expressions of Equation (5) for the parameters listed in the first row of Table 1. GSR, graphene split-ring.

corresponding electric and magnetic polarizability densities defined as:

$$\tilde{P} = \frac{\alpha_{yy}^{EE}}{D^2} \tag{6a}$$

$$\tilde{M} = \frac{\alpha_{zy}^{ME}}{D^2} \tag{6b}$$

RESULTS AND DISCUSSION

The results obtained by Equation (5) are shown in Figure 2b and 2c (dashed curves), together with the results of the numerical simulations for the polarizability densities (solid curves). The fitted parameters $A^{E,M}$ and $B^{E,M}$ were independent of frequency, ring size, graphene quality, and doping; therefore, we used Equation (5) to analyze a wide range of GSR conditions. The fitting values of $A^{E,M}$, $B^{E,M}$ and η_p are given in Table 1 for GSRs with their representative geometrical aspect ratios.

Table 1 The fitting parameters $A^{E,M}$, $B^{E,M}$ and η_p in the analytical expressions Equations (3) and (5) for GSRs with representative values of the aspect ratios (Figure 1a)

W/D	g/D	A^E	B^E	A^M	B^M	A^M/A^E
0.1	0.1	0.0273	0.0226	0.137	−0.064	5
0.2	0.1	0.0216	0.0257	0.099	−0.05	4.6
0.1	0.2	0.033	0.0181	0.139	−0.064	4.2

Abbreviation: GSR, graphene split-ring.

We were interested in assessing the capabilities of graphene compared to gold, which is generally regarded as an excellent standard for metamaterial structures. We considered the performance of split-rings fabricated on four different types of thin films: single-layer and stacked (in which layers can be separated by dielectric spacers[24]) graphene versus single-layer (one (111) atomic layer) and thin-film (20 nm) gold, respectively. For sufficiently thin structures (thickness $t<<D$), the Drude conductivity given by Equation (1) in combination with Equation (5) remains applicable. Expressing the parameter a in terms of the bulk plasma frequency as $a=\omega_{\text{bulk}}^2 t/4\pi$ is convenient. In stacked graphene, an effective bulk frequency $\omega_{\text{bulk}}=(2e/\hbar)\sqrt{E_F/d_z}$ was obtained by simply multiplying the graphene conductivity by the number of graphene layers. Here, d_z is the distance between those layers. Single-layer graphene is retrieved for $t=d_z$. Considering $d_z=2$ nm and $E_F=0.5$ eV, we find that $\hbar\omega_{\text{bulk}}\approx 1.2$ eV, compared with ~9 eV for gold.[25] Obviously, there is some flexibility to reach lower ω_{bulk} values for graphene by simply increasing the interlayer spacing d_z. In addition, the intrinsic damping of gold is $\hbar\gamma\approx 70$ meV, compared with $\hbar\gamma\approx 1$ meV in graphene

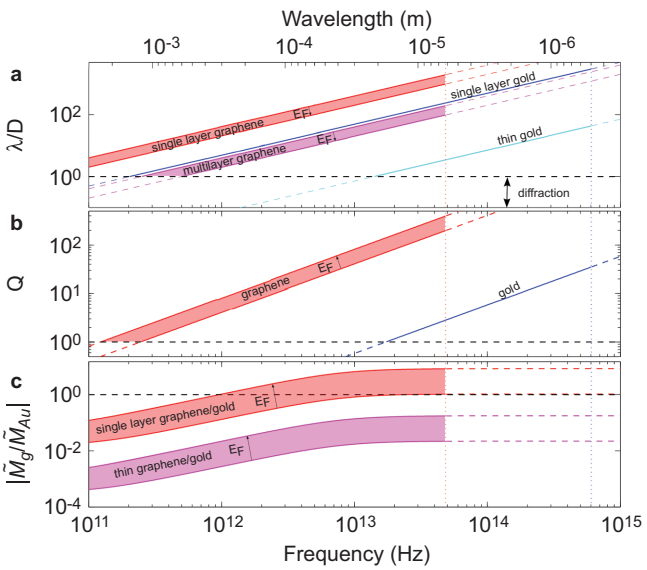

Figure 3 (**a**) The confinement factor and (**b**) the quality factor for single-layer graphene (red), single- atomic-layer gold (thickness t=0.29 nm, blue), 20-nm gold film (thin gold, cyan) and 10 layers of stacked graphene with an interlayer spacing of 2 nm (multilayer graphene, magenta). (**c**) The ratio of the magnetic polarizability density of graphene $\tilde{M}_g$ to that of gold, $\tilde{M}_{\text{Au}}$. Red corresponds to the ratio of monolayers of the two materials, while magenta refers to the ratio of stacked graphene to thin gold. The solid regions spanned by graphene correspond to a Fermi energy range of 0.5–1 eV. The loss thresholds associated with optical phonons in graphene at energies >0.2 eV and with interband transitions in gold at energies greater than 2.5 eV are indicated by the vertical dotted lines. The quality factor in (**b**) is independent of the thickness. Gold is described based on its measured permittivity.[25]

for the levels of doping and mobility under consideration. Therefore, graphene should allow us to operate well at lower energies than gold.

We compared the performances of these types of thin films (Figure 3). In particular, we examined the degree of confinement (Figure 3a), quantified through the ratio of the resonance wavelength to the ring diameter (λ/D), the quality factor $Q=\omega_p/\gamma$ (Figure 3b), and the ratio of the magnetic polarizability density $\tilde{M}$ of monolayer (stacked) graphene over that of monolayer (thin) gold. We set the aspect ratios to $W/D=g/D=0.1$, and we used these expressions with the ring diameter required to obtain the resonance frequency ω_p running along the horizontal axis (Equation (3)). Namely,

$$D=t\left(\omega_{\text{bulk}}\Big/\omega_p\right)^2\Big/\left(4\pi\eta_p\right) \tag{7}$$

Considering the realistic mobilities assumed here ($\mu\approx 13\,000$ cm^2 V^{-1} s^{-1}),[26,27] graphene offers a suitable alternative to fabricate resonant split-rings with $Q>1$ down to the THz regime (Figure 3b) with a degree of confinement that is greater than what is achieved by noble metals for similar thicknesses and frequencies (Figure 3a). In fact, at far-IR wavelengths (longer than 100 μm), the confinement factor for thin gold is smaller than one. This finding indicates that in contrast to stacked graphene, thin gold SRR arrays lie in the diffraction rather than in the metamaterial regime, whereas the corresponding quality factor is much smaller than 1. A comparison between the magnetic response of single-layer gold and single-layer graphene reveals that doped single-layer graphene can provide a stronger magnetic response than single-layer gold at frequencies higher than ~1 THz. The difference between these two materials nearly reaches an order of magnitude when considering strongly doped graphene. The magnetic responses of monolayer and stacked graphene are considerably weaker than the response of thin gold. However, this picture could significantly improve with the availability of higher mobility graphene[28] subjected to stronger doping.[29,30]

CONCLUSIONS

In conclusion, graphene has emerged as a tunable material that allows the fabrication of ultrathin metamaterials. A central element of these metamaterials (split-rings) is shown here, displaying resonances with unprecedented levels of field confinement. Thus, graphene monolayers can be used to reach the true homogenization limit ($D<<\lambda$) with the additional advantage of having an electrically tunable optical response, which can be beneficial for the fabrication of compact, versatile metamaterials down to the terahertz regime.

ACKNOWLEDGMENTS

This work has been supported by the Spanish MICINN (MAT2010-14885 and Consolider NanoLight.es), the European Commission (FP7-ICT-2009-4-248909-LIMA and FP7-ICT-2009-4-248855-N4E), the EPSRC (UK) and the Leverhulme Trust and the MOE Singapore (grant MOE2011-T3-1-005).

1 Smith DR, Pendry JB, Wiltshire MC. Metamaterials and negative refractive index. *Science* 2004; **305**: 788–792.
2 Yen TJ, Padilla WJ, Fang N, Vier DC, Smith DR *et al*. Terahertz magnetic response from artificial materials. *Science* 2004; **303**: 1494–1496.
3 Grigorenko AN, Geim AK, Gleeson HF, Zhang Y, Firsov AA *et al*. Nanofabricated media with negative permeability at visible frequencies. *Nature* 2005; **438**: 335–338.
4 Pendry JB. Negative refraction makes a perfect lens. *Phys Rev Lett* 2000; **85**: 3966–3969.
5 Schurig D, Mock JJ, Justice BJ, Cummer SA, Pendry JB *et al*. Metamaterial electromagnetic cloak at microwave frequencies. *Science* 2006; **314**: 977–980.
6 Wiltshire MC, Pendry JB, Young IR, Larkman DJ, Gilderdale DJ *et al*. Microstructured magnetic materials for RF flux guides in magnetic resonance imaging. *Science* 2001; **291**: 849–851.
7 Enkrich C, Wegener M, Linden S, Burger S, Zschiedrich L *et al*. Magnetic metamaterials at telecommunication and visible frequencies. *Phys Rev Lett* 2005; **95**: 203901.
8 Boudarham G, Feth N, Myroshnychenko V, Linden S, García de Abajo FJ *et al*. Spectral imaging of individual split-ring resonators. *Phys Rev Lett* 2010; **105**: 255501.
9 West P, Ishii S, Naik GV, Emani NK, Shalaev VM *et al*. Searching for better plasmonics materials. *Laser Photonics Rev* 2010; **4**: 795–808.
10 Tassin P, Koschny T, Kafesaki M, Soukoulis CM. A comparison of graphene, superconductors and metals as conductors for metamaterials and plasmonics. *Nat Photon* 2012; **6**: 259–264.
11 Jablan M, Buljan H, Soljacic M. Plasmonics in graphene at infrared frequencies. *Phys Rev B* 2009; **80**: 245435.
12 Koppens FH, Chang DE, García de Abajo FJ. Graphene plasmonics: a platform for strong light–matter interactions. *Nano Lett* 2011; **11**: 3370–3377.
13 Wunsch B, Stauber T, Sols F, Guinea F. Dynamical polarization of graphene at finite doping. *New J Phys* 2006; **8**: 318.
14 Hwang EH, Das Sarma S. Dielectric function, screening, and plasmons in two-dimensional graphene. *Phys Rev B* 2007; **75**: 205418.
15 Fei Z, Andreev GO, Bao W, Zhang LM, McLeod AS *et al*. Infrared nanoscopy of Dirac plasmons at the graphene–SiO_2 interface. *Nano Lett* 2011; **11**: 4701–4705.
16 Ju L, Geng B, Horng J, Girit C, Martin M *et al*. Graphene plasmonics for tunable terahertz metamaterials. *Nat Nanotech* 2011; **6**: 630–634.
17 Fang ZY, Thongrattanasiri S, Schlather A, Liu Z, Ma LL *et al*. Gated tunability and hybridization of localized plasmons in nanostructured graphene. *ACS Nano* 2013; **7**: 2388–2395.
18 Chen J, Badioli M, Alonso-González P, Thongrattanasiri S, Huth F *et al*. Optical nano-imaging of gate-tunable graphene plasmons. *Nature* 2012; **487**: 77–81.
19 Fei Z, Rodin AS, Andreev GO, Bao W, McLeod AS *et al*. Gate-tuning of graphene plasmons revealed by infrared nano-imaging. *Nature* 2012; **487**: 82–85.
20 Thongrattanasiri S, Manjavacas A, García de Abajo FJ. Quantum finite-size effects in graphene plasmons. *ACS Nano* 2012; **6**: 1766–1775.
21 Thongrattanasiri S, Silveiro I, García de Abajo FJ. Plasmons in electrostatically doped graphene. *Appl Phys Lett* 2012; **100**: 201105.
22 Christensen J, Manjavacas A, Thongrattanasiri S, Koppens FHL, García de Abajo FJ. Graphene plasmon waveguiding and hybridization in individual and paired nanoribbons. *ACS Nano* 2012; **6**: 431–440.
23 Ouyang F, Isaacson M. Surface plasmon excitation of objects with arbitrary shape and dielectric constant. *Philos Mag B* 1989; **60**: 481–492.
24 Yan H, Li X, Chandra B, Tulevski G, Wu Y *et al*. Tunable infrared plasmonic devices using graphene/insulator stacks. *Nat Nanotech* 2012; **7**: 330–334.
25 Johnson PB, Christy RW. Optical constants of the noble metals. *Phys Rev B* 1972; **6**: 4370–4379.
26 Novoselov KS, Geim AK, Morozov SV, Jiang D, Zhang Y *et al*. Electric field effect in atomically thin carbon films. *Science* 2004; **306**: 666–669.
27 Novoselov KS, Geim AK, Morozov SV, Jiang D, Katsnelson MI *et al*. Two-dimensional gas of massless Dirac fermions in graphene. *Nature* 2005; **438**: 197–200.
28 Bolotin KI, Sikes KJ, Jiang Z, Klima M, Fudenberg G *et al*. Ultrahigh electron mobility in suspended graphene. *Solid State Commun* 2008; **146**: 351–355.
29 Chen CF, Park CH, Boudouris BW, Horng J, Geng B *et al*. Controlling inelastic light scattering quantum pathways in graphene. *Nature* 2011; **471**: 617–620.
30 Khrapach I, Withers F, Bointon TH, Polyushkin DK, Barnes WL *et al*. Novel highly conductive and transparent graphene-based conductors. *Adv Mater* 2012; **24**: 2844–2849.